Temporal constraints on linear BRDF model parameters

Article

Accepted Version

Temporal constraints on linear BRDF model parameters

Tristan Quaife and Philip Lewis

Abstract

Linear models of BRDF are useful tools for understanding the angular variability of surface reflectance as observed by medium resolution sensors such as MODIS. These models are operationally used to normalise data to common view and illumination geometries and to calculate integral quantities such as albedo. Currently, to compensate for noise in observed reflectance these models are inverted against data collected during some temporal window for which the model parameters are assumed to be constant. Despite this the retrieved parameters are often noisy for regions where sufficient observations are not available. This paper demonstrates the use of Lagrangian multipliers to allow arbitrarily large windows and at the same time produce individual parameter sets for each day even for regions where only sparse observations are available.

Index Terms

BRDF, MODIS, Terra, Aqua.

I. Introduction

Kernel–driven linear Bi-directional Reflectance Distribution (BRDF) models are operationally inverted to provide information about photon scattering processes occurring at the Earth's surface [1]. Such models form the basis of the joint Terra and Aqua Moderate Resolution Imaging Spectrometer (MODIS) BRDF/Albedo product (MCD43) [2], [3]. The MCD43 product uses the Ross–Thick and Li–Sparse kernels to model scattering from volumetric and geometric media respectively along with an isotropic kernel whose value is unity [4]. The primary use of these

The authors are with the NERC National Centre for Earth Observation, Carbon Theme, Department of Geography, University College London, Gower Street, London, WC1E 6BT. UK.

models has been in normalising remote sensing data to common view–illumination geometries and providing estimates of hemispherical integral quantities such as albedo [5]. More recently, the ability of such models to explain variability in the observed reflectance signal have enabled the development of advanced algorithms for detecting change in the land surface, such as burned area mapping [6], and tracking the evolution surface albedo [7], [8].

Despite their ability to explain the observed reflectance the temporal trajectories of retrieved kernel weights are often noisy. This is due in part to high correlations between the kernels at angular sampling typical of medium resolution sensors such as MODIS [9]. For many areas of the land surface this is exacerbated by large numbers of observations lost to cloud cover [10]. Various approaches have been employed or proposed to address these issues, such as varying the size of the temporal window [6], biased estimation techniques [7] and applying temporal functions to the kernel weights [11], [12] or to the observations themselves [13].

This paper examines the use of Lagrangian multipliers to constrain linear BRDF model inversions by imposing conditions of temporal smoothness on the derived kernel weights [14]. The method is widely employed in the atmospheric remote sensing community where it is used to constrain vertical profiles of retrieved atmospheric properties [15]–[18]. By applying Lagrangian multipliers the extent of the temporal window used for inversion may be extended to an arbitrarily large size whilst relaxing the condition that the kernel weights are constant over this time period. In the current paper a window size of one year is used and distinct parameter sets are retrieved for every day. This permits more accurate tracking of events on the surface such as snow melt and vegetation phenology. Furthermore the method allows for kernel weights to be retrieved even for periods where there are only very sparse observations.

From a starting point of Tikhonov regularisation a closely related technique has been employed to constrain linear BRDF model inversions for the case where the the number of observations is fewer than the number of kernels [19], [20]. This method does not employ a constraint of temporal smoothness but a concept of smoothness within parameter space. The justification for this is unclear however. The idea that parameters should evolve smoothly with time on the other hand seems reasonable, and is the approach applied here.

The Kalman filter has been used as a means of applying temporal constraints to the kernel inversion within some time window, based on previous inversions [21]. This technique requires careful parameterisation however and only takes into account previous reflectance samples and

not those from future points in the time series. Consequently the retrieved kernel weight profiles exhibit sharp changes when observations are available. This later point could be addressed by applying a Kalman smoother (KS) [22], [23] in place of the Kalman filter. The method developed in this paper is shown to be functionally equivalent to the Kalman smoother and through its derivation it is possible to explain the physical meaning of the Kalman parameters for the somewhat abstract concept of a kernel weight process model.

II. Constrained linear inversion

Linear Bi-dectional Reflectance Factor (BRF) models are of the general form:

$$\rho(\Omega, \Omega', \lambda) = \sum_{j=1}^{n} f_j(\lambda) K_j(\Omega, \Omega') \tag{1}$$

where ρ is the BRF at wavelength λ and viewing and illumination geometries Ω and Ω' respectively. K_j are kernels that describe the variation of reflectance with the veiwing and illumination geometry and f_j are kernel weights that describe the contribution of each kernel at a given wavelength. The number of kernels used is denoted n, typically 3. For a vector $\boldsymbol{\rho}$ of m reflectance values (1) can be expressed in matrix notation as:

$$\boldsymbol{\rho} \;=\; \mathbf{K}\mathbf{f} \tag{2}$$

where $\mathbf{f}$ is an n length vector of kernel weights and $\mathbf{K}$ is a $m \times n$ matrix of kernel values. Given observations of reflectance at known angles it is possible to invert (2) to provide estimates of the kernel weights. If the number of observations is greater than the number of kernels (*i.e.*, $m > n$) then least squares methods may be used to minimise the impact of observation errors.

A. Standard least squares solution

The least squares solution to (2), for the overdetermined case, is obtained by:

$$\mathbf{f} \;=\; \left(\mathbf{K}^T\mathbf{C}^{-1}\mathbf{K}\right)^{-1}\mathbf{K}^T\mathbf{C}^{-1}\;\boldsymbol{\rho} \tag{3}$$

where ^{T} denotes a matrix transpose, $^{-1}$ denotes matrix inversion and $\mathbf{C}$ is the observation covariance matrix. For view–illumination geometries typical of medium resolution sensors such as Terra and Aqua MODIS, (3) must be applied across some time window so that sufficient

samples are collected to solve for model parameters and compensate for noise in the observations. In the MOD43 BRDF/albedo product, which uses data from only Terra-MODIS, this window is set to 16 days. In the MCD43 product that uses data from both Terra and Aqua MODIS this window is 8 days. The underlying assumption is that $\mathbf{f}$ does not change within that time period.

B. Constrained least squares solution

It is possible to modify (3) so as to impose an expectation of the temporal behaviour of the kernel weights [18]:

$$\begin{aligned} \mathbf{f}^* &= \left(\mathbf{K}^{*T}\mathbf{C}^{-1}\mathbf{K}^* + \mathbf{B}^T\mathbf{\Gamma}^2\mathbf{B}\right)^{-1} \cdot \\ &\quad \left(\mathbf{K}^{*T}\mathbf{C}^{-1}\ \boldsymbol{\rho}\ + \mathbf{B}^T\mathbf{\Gamma}^2\mathbf{q}\right) \end{aligned} \tag{4}$$

where $\mathbf{B}$ specifies the required constraint, and $\mathbf{\Gamma}$ is a weighting operator, with $\mathbf{\Gamma}^2 = \mathbf{\Gamma}^T\mathbf{\Gamma}$. This provides the solution to the least squares problem in (2) subject to the constraint $\mathbf{Bf}^* = \mathbf{q}$. To impose a condition of temporal smoothness on the kernel weights $\mathbf{B}$ is set to a first difference matrix, $\mathbf{q}$ is set to zero and $\mathbf{\Gamma}$ is set to the product of the identity matrix and a scalar, γ. In this context γ is a Lagrange multiplier. The general constraint (4) becomes:

$$\mathbf{f}^* = \left(\mathbf{K}^{*T}\mathbf{C}^{-1}\mathbf{K}^* + \gamma^2\mathbf{B}^T\mathbf{B}\right)^{-1}\mathbf{K}^{*T}\mathbf{C}^{-1}\ \boldsymbol{\rho} \tag{5}$$

which is the same formulation as provided by [14]. The Lagrange multiplier, γ, can be interpreted as a measure of confidence in the assumption that the first differences of the model parameters between adjacent days should be zero. This is illustrated by analogy with Kalman smoother below.

Unlike $\mathbf{f}$ the vector $\mathbf{f}^*$ does not refer to an instantaneous realisation of the kernel weights that is assumed to be uniform across some time window. It is an array of kernel weights with one realisation for each time step:

$$\mathbf{f}^* = \begin{bmatrix} f_{1,1} \\ \vdots \\ f_{1,t} \\ f_{2,1} \\ \vdots \\ f_{n,t} \end{bmatrix} \tag{6}$$

where t is the total number of time steps. The time step (δt) may be set to any size over which it is sensible to expect variation in the kernel weights. In the current paper $\delta t = 1$ day and $n = 3$ kernels (*i.e.,* isotropic, Ross–Thick and Li–Sparse). If there is no more than one observation per day then the matrix $\mathbf{K}^*$ is given by:

$$\mathbf{K}^* = \begin{bmatrix} K_1(\Omega_1, \Omega_1') & & \\ & \ddots & \\ & & K_1(\Omega_m, \Omega_m') \\ K_2(\Omega_1, \Omega_1') & & \\ & \ddots & \\ & & K_2(\Omega_m, \Omega_m') \\ \vdots & \vdots & \vdots \\ K_n(\Omega_1, \Omega_1') & & \\ & \ddots & \\ & & K_n(\Omega_m, \Omega_m') \end{bmatrix} \tag{7}$$

If there are no observations for some time step then the corresponding kernel values are replaced with zeros. In this case, or where there is exactly one observation per time step the number of rows in the matrix will be nt. If there is more than one observation for a time step then the additional kernel values are placed directly underneath the corresponding kernels for that time step *i.e.,* off the diagonal. In this case the number of rows is $nt + p$ where p is the total number of observations greater than one for a time step, summed across all time steps. The number of columns in $\mathbf{K}^*$ is always t.

The $nt \times nt$ matrix $\mathbf{B}$ defines the constraint of first differences:

$$\mathbf{B} = \begin{bmatrix} 0 & 0 & & & \\ -1 & 1 & 0 & & \\ 0 & -1 & 1 & 0 & \\ & \ddots & \ddots & \ddots & \ddots \\ & & 0 & -1 & 1 & 0 \\ & & & 0 & -1 & 1 \end{bmatrix} \tag{8}$$

where every $t^{th}+1$ row is set to zero. This prevents the constraint being applied across the end of the time series for one kernel to the beginning of the next.

C. Determination of γ

There is very little consent in the literature as to how the value of γ should be selected. The approach taken here is to select a value that produces residuals whose standard deviation is equal to the expected error in the reflectance data. For band one this is equal to 0.004 and for band two it is 0.015 [6]. Consequently the RMSE of predicted to observed reflectance is pre–determined and cannot be used as a measure of goodness of fit.

Although this approach appears to give good results from the perspective of the temporal trajectories of the retrieved kernel weights the value of γ itself is quite variable both spatially and spectrally when determined in this manner. In addition some iteration is required to obtain the required value. Clearly an analytical means of determining γ would be preferable; this has not been pursued here.

III. RESULTS

A. Simulations

[FIGURE 1 ABOUT HERE]

To test the method, hypothetical temporal trajectories of the BRDF kernels were created and used to simulate reflectance values. MODIS angular sampling for a typical mid–latitude site was used for the simulations, in this case the Barton Bendish EOS core validation site at 52.618° latitude, 0.524° longitude [24]. The site is dominated by cereal crops and sugar beet and typical field size is small compared to the resolution of the MODIS sensor. Consequently pixels generally contain mixed agricultural cover types. The kernel weights were inverted against the

simulated reflectances using the method described above and following this against the same data with varying amounts of noise added and samples removed to represent realistic scenarios for medium resolution satellite data.

Fig. 1 shows the results for the constrained linear inversion (5) and a 16–day moving window where 60% of reflectance samples have been removed and Gaussian noise has been added into the simulated data with a standard deviation of 0.015. The smoothness constraint clearly does a better job of reconstructing the original signal, especially for the volumetric kernel. It also appears to be more robust to local outliers than the moving window approach. It should be noted that in the actual MODIS BRDF/albedo the 'magnitude inversion' method is invoked if there is not sufficient good quality data to produce a reliable 'full' inversion [25]. As more samples are used in the inversion and less noise is added into the data both methods fit better to the data. With all samples present and no noise both techniques retrieve the hypothetical kernel weights perfectly. As noise is added they all begin to deviate, however the smoothness constraint appears remarkably robust to the removal of samples compared to the 16–day window (results not shown).

[FIGURE 2 ABOUT HERE]

[FIGURE 3 ABOUT HERE]

B. MODIS data

The technique is applied here to MODIS data for two different regions. The MOD09 and MYD09 500m surface reflectance products from the Terra and Aqua MODIS instruments (respectively) were filtered using their internal QA flags to provide reflectance samples. The results were compared against the combined Terra and Aqua BRDF/albedo product MCD43, which is produced on an 8–day moving window basis. These are shown in Fig. 2 and 3. Kernel weights produced by magnitude inversion [25], or for which no inversion was performed for the MCD43 product are indicated in the results figures as grey bars.

1) MODIS tile h17v04: Fig. 2 shows results for a pixel in Northern Spain, latitude 43.025, longitude -6.674, an area of deciduous forest. The phenological signal is clear in both band 1 and band 2 with leaf–out occurring between day 100 and 150 marked in the isotropic kernel weight by a decline in red band and an increase in the near infra–red. Senescence appears to

be a longer processes and is marked by a gradual decline in the near infra–red isotropic kernel weight and no appreciable signal change in the red channel.

The volumetric kernel weights produced by the smoothness constraint are considerably less noisy than those in the MCD43 product, as predicted by the simulation results. This is especially so in band 1. Intriguingly, in band 2, the constrained volumetric kernel weight exhibits a clear phenological signal that is not readily distinguished in the MCD43 data. This fits the expectation of photon scattering in the canopy, where near infra–red light will be scattered strongly by an abundance of green leaves. There is no clear signal in the geometric kernel for either the smoothness constraint or the MCD43 kernel weights.

2) MODIS tile h23v03: The pixel represented in Fig. 3 is deciduous forest in Siberia, latitude 52.906, longitude 86.968. The temporal signal in this pixel is more complex as there are two processes effecting the reflectance: vegetation phenology and snow presence. In addition the number of reflectance samples available in the winter months is very low forcing the use of magnitude inversion for approximately half of the MCD43 data. At the very end of the year there are no samples at all so neither method produces any results. In the case of the constrained inversion increasing the time window up to the point where some observation were available would result in estimates of the kernel weights for the entirety of this time period. This is not possible with the MCD43 alogrithm.

The influence of snow is very clear in these inversions. Both the near infra–red and red reflectances are very high for around the first 100 days of the year. After this the snow begins to melt, resulting in decreasing reflectance, but then leaves start to flush and and the near infra–red reflectance increases. During the middle of the year both methods agree well for the isotropic and geometric kernel weights. As with the previous example, however, the volumetric kernel weights do not correspond well between the two methods. The constrained volumetric kernel weights in band 2 exhibit a similar temporal profile to those from the pixel in tile h17v04.

During the periods for which the MCD43 product uses magnitude inversions, or produces no data, the constrained inversion pushes the geometric kernel weight slightly negative. This could be addressed by adding further constraints into the inversion.

C. Predicting Aqua MODIS data from Terra MODIS

By adjusting γ the reflectance data used to fit the kernel weights can be predicted with arbitrary accuracy. Consequently to test the fitting of the BRDF model it is necessary to exclude some data from the constrained least squares procedure and use these to evaluate the performance of the method. Fig. 4 shows the results of fitting the kernel weights to Terra MODIS reflectance data and then predicting the observed Aqua MODIS reflectance. In this circumstance it is acceptable to calculate metrics such as the Root Mean Squared Error (RMSE), as the test data has not been used in the model fitting or the determination of γ. Excluding a single outlier in the Aqua reflectance data the RMSE is 0.0058 and 0.0296 for band 1 and band 2 respectively for tile h17v04. In band 1 this corresponds to 26% of the mean observed reflectances, and 13% in band 2. The data appear to lie evenly around the 1:1 line and exhibit only a small negative bias in both bands, -0.0016 in band 1 and -0.0039 in band 2. The Aqua observations have slightly higher values than those modelled from the Terra data. For tile h23v03 the prediction is much stronger. The RMSE values are 0.0051 and 0.0117 for bands 1 and 2 respectively, corresponding to a 15% in band one and 4% in band 2.

[FIGURE 4 ABOUT HERE]

D. Functional equivalence with the Kalman smoother

[FIGURE 5 ABOUT HERE]

Fig. 5 shows the kernel weights for MODIS band 2 retrieved using constrained inversion, as shown in Fig. 2b, superimposed with the results for a Kalman smoother applied to the same data. The KS requires some concept of an underlying process model that controls the evolution of the kernel weights with time. In this case the model used is a zero–order model, *i.e.*, there is no expected change in the kernel weights with time. This is conceptually similar to constraining the first differences to be as small as possible, *i.e.*, by defining $\mathbf{B}$ as in (8) and setting $\mathbf{q}$ to zero.

A common difficulty with utilising the KS is setting the error term for the process model. In previous work utilising the kernel BRDF models with a Kalman filter and a zero order process model it has been set arbitrarily [21]. In Fig. 5 the error term for the KS has been given a value of $1/\gamma^2$ corresponding to that used for the Lagrangian multiplier in the constrained inversion. Although the results are not identical, they are very similar and differences could be due to computational precision: the constrained inversion requires one large matrix inversion

and the KS requires many small matrix inversions. Using the same value of γ for both the KS and the constrained inversion demonstrates that the Lagrange multiplier may be interpreted as the certainty in the underlying assumption of smoothness. This suggest a functional equivalence between the two methods, although it is not proved here. Consequently the constrained inversion outlined in this paper may have applications in the field of data assimilation.

IV. Discussion

The approach of using Lagrangian multipliers to constrain the inversions clearly works well. By allowing for a large time window the angular sampling is much increased and inversions with greater stability are produced. Both phenology and snow melt in the results shown for Northern Spain and Siberia are well described by the method. These are attractive features for such a technique as the size of windows typically used for BRDF model inversions can reduce the accuracy with which the timing of such events is detected. Attempting to track such changes with surface reflectance, or even vegetation indicies can be difficult without taking into account the variability in reflectance caused by changes in viewing and illumination geometry: the magnitude in the angular signal may be significant in terms of that induced by the change in surface properties.

Step changes in the reflectance signal, such as burning of surface vegetation or flash flooding, may not be as well detected because they are not smooth. However, it may be able possible to adapt the technique to deal with such situations by applying more elaborate constraints using different formulations of $\mathbf{B}$, $\mathbf{\Gamma}$ and $\mathbf{q}$ [26]. For example, this may entail an iterative approach to building of the $\mathbf{\Gamma}$ matrix. At times when the signal is changing rapidly the elements of $\mathbf{\Gamma}$ can be relaxed to allow the parameters to respond more quickly.

In aerosol profile retrieval problems it is common to use a second difference constraint rather than first differences, as here. Second differences were tried with the BRDF model inversions but first differences gave more satisfactory results, especially towards either end of the time series. It is worth noting that (4) can be extended with multiple constraint matrices allowing for complex models of expectation in the temporal evolution of the kernel weights. It is also possible to add constraints that prevent the kernel weights from going negative (as with the MCD43 algorithm). An additional example of a modified constraint that is straight forward to apply, is to have separate γ for each kernel.

The method for selecting γ requires further investigation. Here the approach taken has been to select a value that produces appropriate residuals, and the resulting kernel weight profiles appear to justify this method. The actual values of γ determined by this mechanism are very variable though. Clearly a more satisfactory solution would be to have an analytical approach to the problem. This is likely to be a function of the angular and temporal sampling and will form the basis of a future study.

Errors in the retrieved kernel weights have not been examined in this paper. These may be estimated directly from the inverse matrix using the same technique as for the weights of determination [9]. As the formulation used in this paper includes the observation covariance matrix the results will be direct estimates of the error rather than the noise amplification factor. This is important as it will permit direct quantification of error in information derived from the kernel weights such as phenological metrics or hemispherical integrals (*e.g.,* albedo).

Although only a single matrix inversion is required to produce kernel weights for an entire year (or more) the size of the matrix is such that no advantage in speed is gained: it is comparable with the KS. Techniques for dealing with large, sparse matrices have not been investigated however and these may provide a computational advantage.

V. Conclusion

This paper has described a method for inverting linear kernel–driven BRDF models using Lagrangian multipliers to impose expectations of temporal smoothness on the resulting kernel weights. The method permits for an arbitrarily large time window for the collection of reflectance observations without assuming that the kernel weights must be constant within this time window. Individual sets of kernel weights can be produced for each time step inside the window. The technique is shown to work well for two different areas of the Earth's surface that both exhibit strong temporal variability due to vegetation phenology and snow. In these cases the window size was set to one year and the time step was set to one day. This negates the requirement for a backup algorithm to retrieve the kernel weights such as the one used in the MCD43 product.

Acknowledgment

This work was funded as part of the UK NERC National Centre for Earth Observation (NCEO), Carbon theme.

REFERENCES

[1] J. Roujean, M. Leroy, and P. Deschamps, "A bidirectional reflectance model of the Earth's surface for the correction of remote sensing data," *Journal of Geophysical Research*, vol. 97, pp. 20 455–20 468, Dec. 1992.

[2] A. H. Strahler, W. Lucht, C. B. Schaaf, T. Tsang, F. Gao, X. Li, J. P. Muller, P. Lewis, M. J. Barnsley, and D. McIver, "MODIS BRDF/Albedo product: Algorithm theoretical basis document version 5.0," *National Aeronautics and Space Administration*, 1999.

[3] C. B. Schaaf, F. Gao, A. H. Strahler, W. Lucht, X. Li, T. Tsang, N. C. Strugnell, X. Zhang, Y. Jin, and J. P. Muller, "First operational BRDF, albedo and nadir reflectance products from MODIS," *Remote Sensing of Environment*, vol. 83, pp. 135–148, Nov. 2002.

[4] W. Wanner, X. Li, and A. H. Strahler, "On the derivation of kernels for kernel-driven models of bidirectional reflectance," *Journal of Geophysical Research*, vol. 100, pp. 21,077–21,089, 1995.

[5] A. Lyapustin, Y. Wang, J. Martonchik, J. Privette, B. Holben, I. Slutsker, A. Sinyuk, and A. Smirnov, "Local analysis of MISR surface BRF and albedo over GSFC and mongu AERONET sites," *Geoscience and Remote Sensing, IEEE Transactions on*, vol. 44, no. 7, pp. 1707–1718, 2006.

[6] D. Roy, Y. Jin, P. Lewis, and C. Justice, "Prototyping a global algorithm for systematic fire-affected area mapping using MODIS time series data," *Remote Sensing of Environment*, vol. 97, pp. 137–162, Jul. 2005.

[7] I. Pokrovsky, O. Pokrovsky, and J.-L. Roujean, "Development of an operational procedure to estimate surface albedo from the SEVIRI/MSG observing system by using POLDER BRDF measurements: I. data quality control and accumulation of information corresponding to the IGBP land cover classes," *Remote Sensing of Environment*, vol. 87, pp. 198–214, Oct. 2003.

[8] ——, "Development of an operational procedure to estimate surface albedo from the SEVIRI/MSG observing system by using POLDER BRDF measurements: II. comparison of several inversion techniques and uncertainty in albedo estimates," *Remote Sensing of Environment*, vol. 87, pp. 215–242, Oct. 2003.

[9] W. Lucht and P. Lewis, "Theoretical noise sensitivity of BRDF - and albedo retrieval from the EOS-MODIS - and MISR - sensors with respect to angular sampling," *International Journal of Remote Sensing*, vol. 21, pp. 81–98, 2000.

[10] D. Roy, P. Lewis, C. Schaaf, S. Devadiga, and L. Boschetti, "The global impact of clouds on the production of MODIS bidirectional reflectance model-based composites for terrestrial monitoring," *Geoscience and Remote Sensing Letters, IEEE*, vol. 3, pp. 452–456, 2006.

[11] L. Rebelo, P. Lewis, and D. Roy, "A temporal-BRDF model-based approach to change detection," in *Proc. IEEE International Geoscience and Remote Sensing Symposium (IGARSS '04)*, vol. 3, 2004, pp. 2103–2106.

[12] E. Vermote, C. Justice, and F. Breon, "Towards a generalized approach for correction of the BRDF effect in MODIS directional reflectances," *Geoscience and Remote Sensing, IEEE Transactions on*, vol. 47, no. 3, pp. 898–908, Mar. 2009.

[13] O. Samain, B. Geiger, and J. Roujean, "Spectral normalization and fusion of optical sensors for the retrieval of BRDF and albedo: Application to VEGETATION, MODIS, and MERIS data sets," *Geoscience and Remote Sensing, IEEE Transactions on*, vol. 44, no. 11, pp. 3166–3179, Nov. 2006.

[14] S. Twomey, *Introduction to the Mathematics of Inversion in Remote Sensing and Indirect Measurements*. Dover Publications, 1996.

[15] R. Rizzi, R. Guzzi, and R. Legnani, "Aerosol size spectra from spectral extinction data: the use of a linear inversion method," *Applied Optics*, vol. 21, pp. 1578–1587, May 1982.

[16] G. E. Shaw, "Inversion of optical scattering and spectral extinction measurements to recover aerosol size spectra," *Applied Optics*, vol. 18, pp. 988–993, Apr. 1979.

[17] M. D. King, "Sensitivity of constrained linear inversions to the selection of the Lagrange multiplier," *Journal of the Atmospheric Sciences*, vol. 39, pp. 1356–1369, Jun. 1982.

[18] D. Feng, "A new formula for the linear constrained matrix inversion," in *Combined Optical, Microwave, Earth and Atmosphere Sensing, 1993., Proceedings of IEEE Topical Symposium on*, 1993, pp. 60–63.

[19] Y. Wang, X. Li, Z. Nashed, F. Zhao, H. Yang, Y. Guan, and H. Zhang, "Regularized kernel-based BRDF model inversion method for ill-posed land surface parameter retrieval," *Remote Sensing of Environment*, vol. 111, pp. 36–50, Nov. 2007.

[20] Y. Wang, C. Yang, and X. Li, "Regularizing kernel-based BRDF model inversion method for ill-posed land surface parameter retrieval using smoothness constraint," *Journal of Geophysical Research*, vol. 113, p. D13101, Jul. 2008.

[21] O. Samain, J.-L. Roujean, and B. Geiger, "Use of a Kalman filter for the retrieval of surface BRDF coefficients with a time-evolving model based on the ECOCLIMAP land cover classification," *Remote Sensing of Environment*, vol. 112, pp. 1337–1346, Apr. 2008.

[22] S. E. Cohn, N. Sivakumaran, and R. Todling, "A fixed-lag kalman smoother for retrospective data assimilation," *Monthly Weather Review*, vol. 122, pp. 2838–2867, Dec. 1994.

[23] S. Sarkka, A. Vehtari, and J. Lampinen, "Time series prediction by Kalman smoother with cross-validated noise density," in *Proc. IEEE International Joint Conference on Neural Networks*, vol. 2, Jul. 2004, pp. 1653–1657.

[24] M. Disney, P. Lewis, G. Thackrah, T. Quaife, and M. Barnsley, "Comparison of MODIS broadband albedo over an agricultural site with ground measurements and values derived from Earth observation data at a range of spatial scales," *International Journal of Remote Sensing*, vol. 25, pp. 5297–5317, Dec. 2004.

[25] W. Lucht, C. B. Schaaf, and A. H. Strahler, "An algorithm for the retrieval of albedo from space using semiempirical BRDF models," *Geoscience and Remote Sensing, IEEE Transactions on*, vol. 38, pp. 977–998, Mar. 2000.

[26] C. F. Youzwishen and M. D. Sacchi, "Edge preserving imaging," *Journal OF Seismic Exploration*, vol. 15, pp. 45–58, 2006.

PLACE PHOTO HERE

Tristan Quaife Tristan Quaife received a B.Sc. in environmental chemistry from the University of Hertfordshire in 1997 and a Ph.D. in remote sensing from the University of Wales Swansea in 2001.

Since 2003 he has held a postdoctoral position at University College London, original in the Centre for Terrestrial Carbon Dynamics and latterly in the National Centre for Earth Observation (Carbon Theme). Both positions were funded by the Natural Environment Research Council. His primary research interest is using data assimilation techniques to interface environmental models with earth observation data.

PLACE PHOTO HERE

Philip Lewis Philip Lewis received a B.Eng. degree in avionics from Queen Mary College, London, 1987. Following these he obtained M.Sc. and Ph.D. degree in remote sensing from University College London in 1988 and 1996 respectively.

He has held a permanent position at University College London since 1992, firstly as a Lecture, then reader and now Professor of remote sensing in the Department of Geography. His research interests are in the monitoring and modelling of vegetation using earth observation data and physically based models. He is a principal investigator on the Carbon Theme of the Natural Environment Research Council (NERC) National Centre for Earth Observation (NCEO).

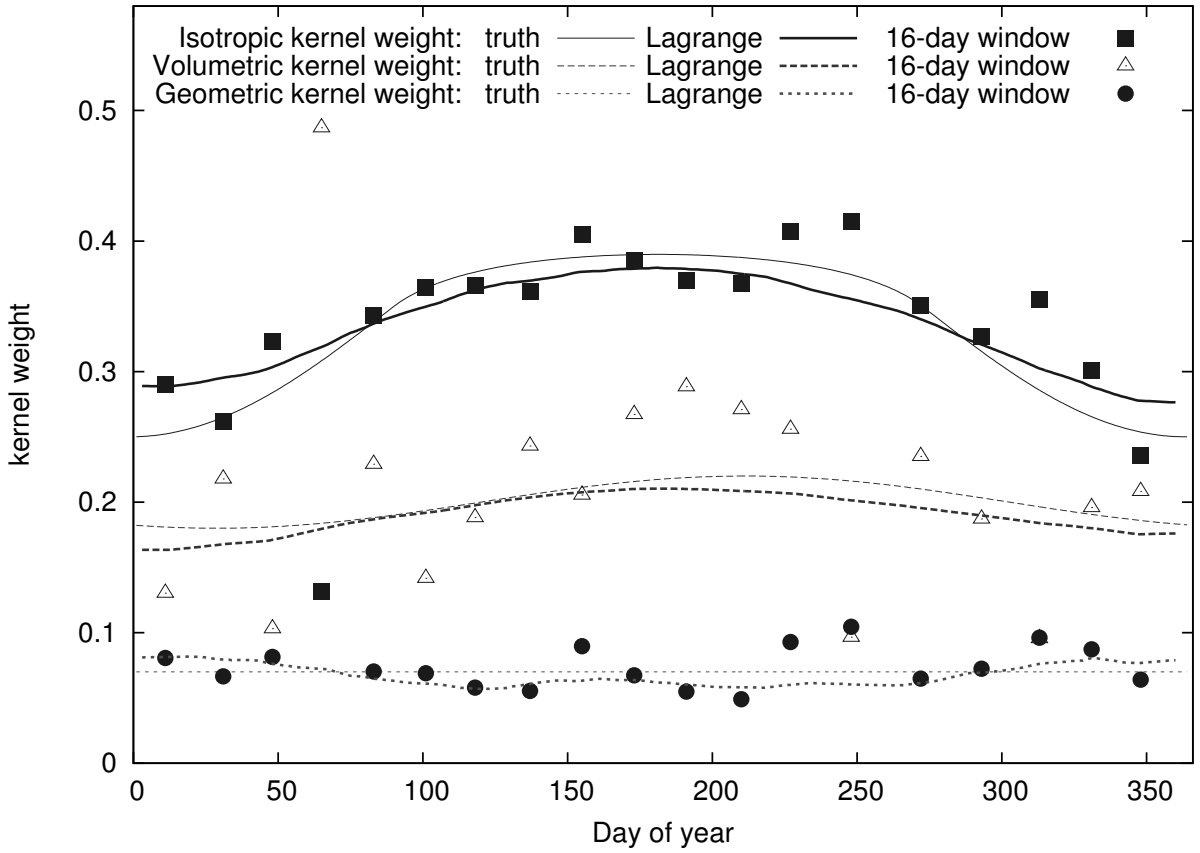

Fig. 1. Simulation results for typical mid–latitude Terra/MODIS angular sampling with gaussian noise added to simulated reflectance at $\sigma = 0.015$ and 60% of samples removed at random. Langrange refers to the constrained inversions.

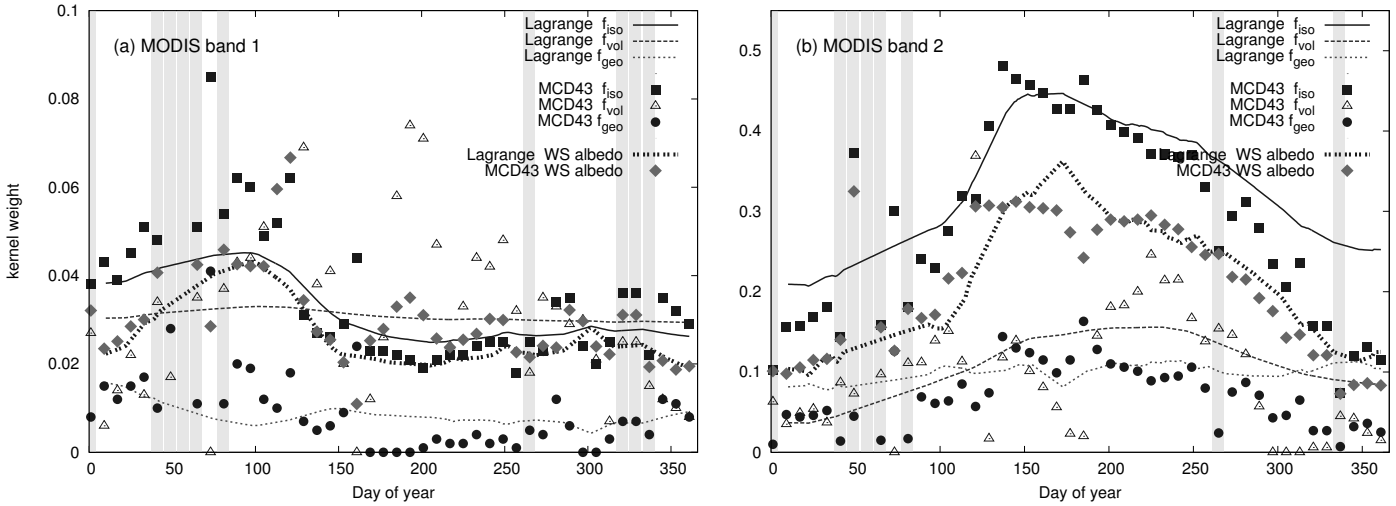

Fig. 2. Temporal trajectories of the kernel weights for MODIS bands 1 and 2 for the pixel in tile h17v04. Lines refer to values obtained using the smoothness constraint and points are taken from the MCD43 product. Grey boxes indicate periods where the MCD43 product has used the magnitude inversion backup algorithm or produced no results at all.

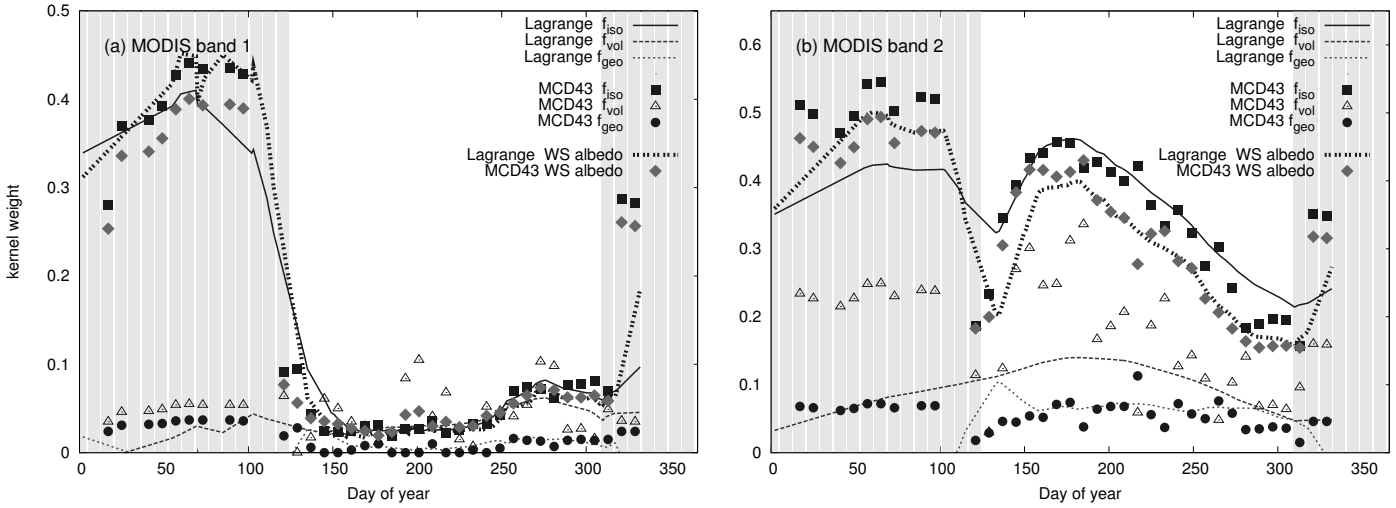

Fig. 3. Temporal trajectories of the kernel weights for MODIS bands 1 and 2 for the pixel in tile h23v03. Lines refer to values obtained using the smoothness constraint and points are taken from the MCD43 product. Grey boxes indicate periods where the MCD43 product has used the magnitude inversion backup algorithm or produced no results at all.

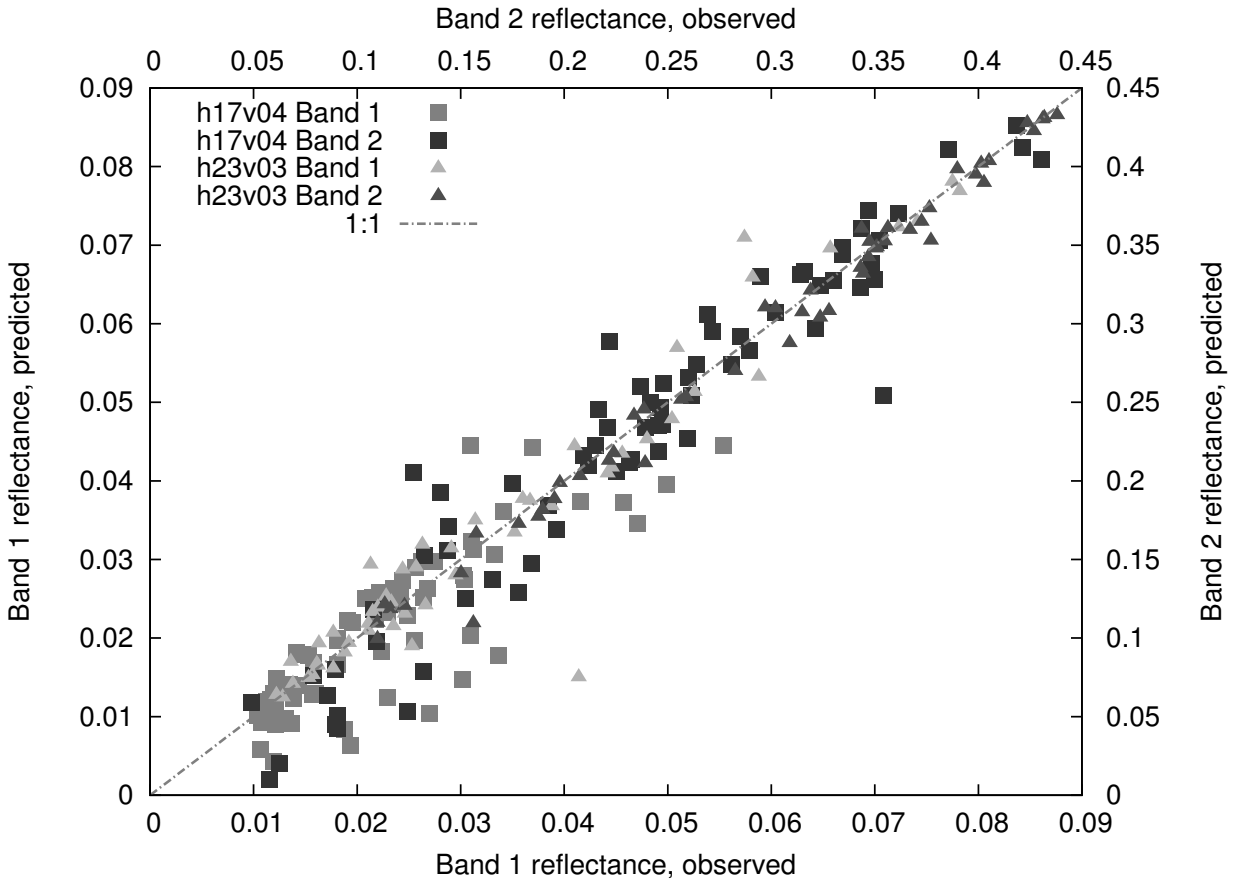

Fig. 4. Scatter plot of Aqua MODIS reflectance predicted from Terra MODIS data using kernel weights derived with the smoothness constraint. One point in band 1 for h17v04 lies out side the range of the plot.

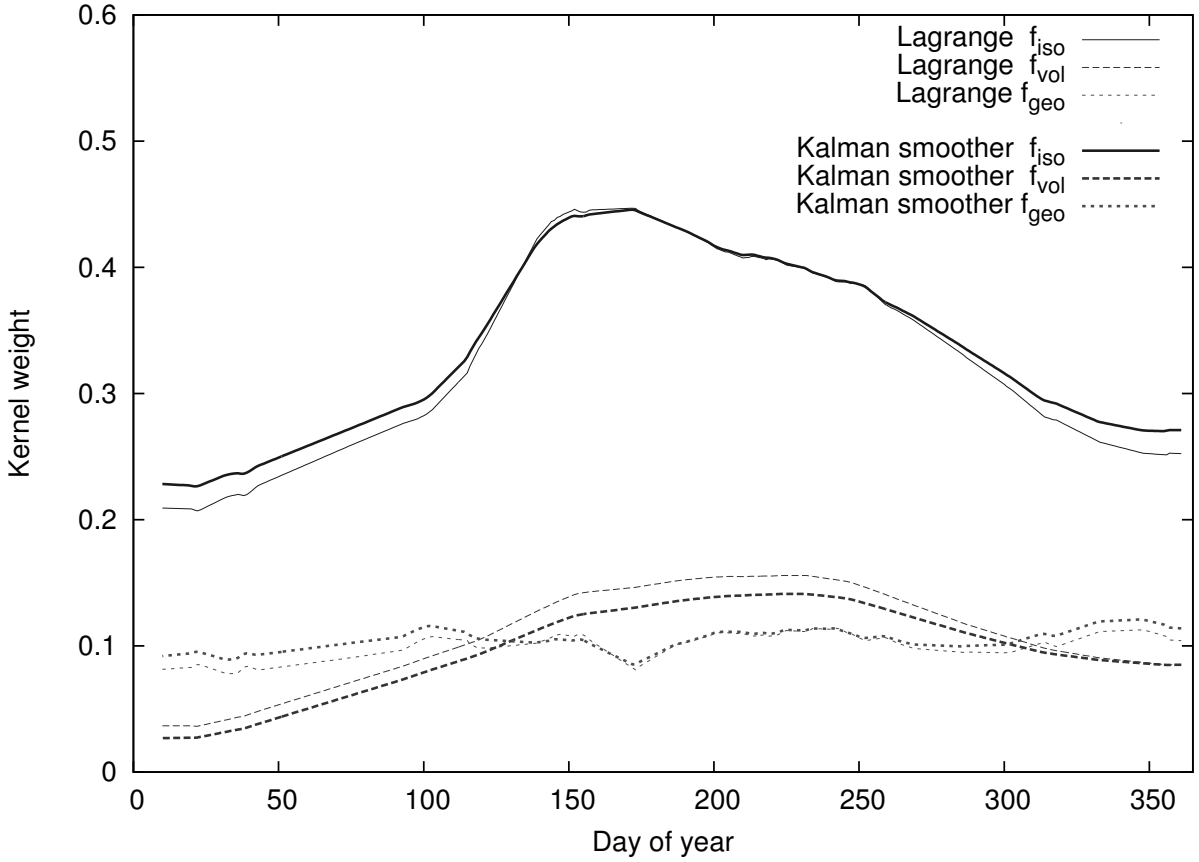

Fig. 5. Constrained linear inversion and Kalman Smoother results for the pixel in tile h17v04, band 2. Coefficient of determination (R^2) values for the kernel weights for the two techniques: isotropic, $R^2 = 0.9994$; volumetric, $R^2 = 0.9871$; geometric $R^2 = 0.7891$.